

Targeted photodynamic therapy with multiply-loaded recombinant antibody fragments

Manpreet Bhatti¹, Gokhan Yahioglu^{2,3*}, Lionel R. Milgrom^{2,3}, Mitla Garcia-Maya¹, Kerry A. Chester⁴ and Mahendra P. Deonarain^{1*}

¹Division of Cell and Molecular Biology, Faculty of Natural Sciences, Imperial College London, Exhibition Road, London, United Kingdom

²PhotoBiotics, 21 Wilson Street, London EC2M 2TD, United Kingdom

³Department of Chemistry, Faculty of Natural Sciences, Imperial College London, Exhibition Road, London, United Kingdom

⁴Department of Oncology, Royal Free and University College Medical School, University College London, London, United Kingdom

Current photodynamic therapy (PDT) of cancer is limited by inefficiencies involved in specifically targeting photosensitizers to tumors. Although antibodies are being explored as targeting vehicles, they present significant challenges, particularly in terms of pharmacokinetics and drug-coupling. We describe here a novel and effective system to covalently attach multiple photosensitizer molecules (both preclinical, pyropheophorbide-*a* and clinically approved, verteporfin photosensitizers) to single-chain Fvs. Further, we demonstrate that not only do the resulting photoimmunoconjugates retain photophysical functionality, they are more potent than either free photosensitizer, effectively killing tumor cells *in vitro* and *in vivo*. For example, treatment of human breast cancer xenografts with a photoimmunoconjugate comprising an anti-HER-2 scFv linked to 8–10 molecules of pyropheophorbide-*a* leads to significant tumor regression. These results give an insight into the important features that make scFvs good carriers for PDT drugs and provide proof of concept of our unique approach to targeted photodynamic therapy (tPDT). This promises to significantly improve on current photodynamic therapies for the treatment of cancer.

© 2007 Wiley-Liss, Inc.

Key words: photodynamic therapy; single chain Fv; pyropheophorbide-*a*; verteporfin

Photodynamic therapy (PDT) is a minimally invasive procedure used in a range of conditions where superficially localized lesions such as age-related macular degeneration (AMD) or tumors need to be treated.¹ PDT is typically a 2-step process that involves the administration of a photosensitizer (PS) leading to marginal accumulation in the tumor. Following this, the PS is activated by exposure to light of an appropriate wavelength. This ultimately leads to the conversion of molecular oxygen into reactive oxygen species (ROS), primarily singlet oxygen, leading to tumor cell death *via* irreversible damage to cellular components such as proteins, lipids and DNA.²

Current clinical use of PDT achieves efficacies similar to conventional therapies but with lower morbidity, simplicity of use and improved functional and cosmetic outcome.^{3,4} PDT has mainly been used where conventional approaches have failed or were unsuitable. These include premalignant dysplastic lesions and noninvasive cancers, which are commonly found in the mucosa of the aerodigestive⁵ and urinary tracts.⁶ Success in treating these types of cancers has been achieved using Photofrin[®],⁷ Levulan[®]⁸ and Foscan[®].⁹ The most successful application of PDT has been for wet age-related macular degeneration (AMD) for which the photosensitizer verteporfin (Visudyne[®]) has been used to destroy ocular neovasculation.¹⁰ PDT has also had great successes in dermatology because of its impressive cosmetic outcome. Methyl 5-aminolaevulinate (Metvix[®]) has been used to treat actinic keratosis with up to 90% cure.¹¹

Although PSs accumulate in cancer cells, the tumor specificity ratios are low and their inherent hydrophobicity, causes them to persist in the circulation for longer than is desired which can leave the patient photosensitive for more than 4 weeks.¹² To improve specificity, PSs have been coupled to targeting elements such as monoclonal antibodies¹³ or other ligands.¹⁴

Photosensitizers conjugated to whole antibodies can target a range of cancers¹² or pathogens¹⁵; however, experiences so far has shown that many technical problems exist in coupling high numbers of PS to whole antibodies. These include impaired antibody binding, reduced solubility^{16–19} and unfavorable pharmacokinetics due to the resulting high molecular weight of such photoimmunoconjugates (PICs). Some researchers have tried using carrier moieties such as branched carbohydrate or polylysine chains, which are in turn linked to the antibody.²⁰ This process requires multiple conjugation steps adding to the complexity of commercial manufacture. A further disadvantage of such carriers is that PSs can end up being in close proximity to each other, quenching their excited states and ultimately reducing the energy available for ROS generation, needed to cause cellular damage.²¹

Antibody fragments such as scFvs (single-chain Fv fragments) have been shown to be superior to whole antibodies in many aspects of tumor targeting such as speed of penetration and tumor:normal tissue specificity,^{22,23} making them ideal vehicles for targeted PDT if sufficient numbers of PS can be attached to these small 30 kDa proteins. Photocoagulation of ocular vasculature²⁴ and tumor destruction²⁵ have been demonstrated by Neri and coworkers using the antibody fragment L19; however, this and other research¹⁷ illustrates the challenge in that only 1–2 PS molecules could be attached directly to L19.

The rapidly internalizing anti-HER 2 (human epidermal growth factor receptor-2) C6.5 scFv²⁶ was selected for evaluation for PDT. This scFv has not previously been conjugated to PSs and HER2 expressing cancers such as breast, head and neck and prostate cancers are diseases that are relevant to PDT.^{27–29} We show here that up to 10 molecules of pyropheophorbide-*a* (PPa) can be coupled directly to 1 molecule of scFv without loss of photophysical activity, which in turn, causes tumor cell death *in vitro* and *in vivo*. We also show the general utility of our approach by improving the potency and selectivity of a successful and commercially approved photosensitizer. Furthermore, using a panel of different scFvs, we discuss the features of recombinant antibodies that enable them to make effective photoimmunoconjugates. This has implications in engineering scFv carriers to control the number and function of the PS that can be coupled.

Material and methods

Materials

Carcinoembryonic antigen was from Calbiochem. *E. coli* BL21 (DE3) and pET20b vector was obtained from Novagen, Notting-

*Correspondence to: Division of Cell and Molecular Biology, Faculty of Natural Sciences, Imperial College London, Exhibition Road, London SW7 2AZ, UK. Fax: +44 207 594 4560.
E-mail: m.deonarain@imperial.ac.uk

Received 25 April 2007; Accepted after revision 7 August 2007

DOI 10.1002/ijc.23206

Published online 31 October 2007 in Wiley InterScience (www.interscience.wiley.com).

ham, UK. Pyropheophorbide-*a* was obtained from Frontier Scientific. Anti-MFE scFv antiserum was raised by the CR-UK (Frontier Scientific, Carnforth, UK) Oncology group (UCL, Rowland Hill Street).

Cell culture

The human tumor cell lines SKOV-3 (HER2+, CEA-), KB (HER2-), WI38(VA13) (EDB fibronectin+) and LoVo (CEA+, HER2-) were obtained from the European Collection of Cell Cultures (ECACC). KB and LoVo cells were cultured in Dulbecco's modified Eagle's medium (DMEM) with 10% fetal calf serum, penicillin and streptomycin antibiotics and passaged when 70–90% confluent in 75 cm² flasks. SKOV-3 cells were cultured in McCoy's 5A medium supplemented with 15% fetal calf serum (FCS), penicillin and streptomycin antibiotics and 0.22 g/l L-glutamine and passaged when 70–90% confluent.

Expression and purification of MFE-23 and C6.5 scFv

The MFE-23 scFv in pUC119³⁰ was recloned into the pET-20b vector as an *Nco* I/*Not* I fragment and the protein expressed in BL21(DE3) cells. Cultures of 500 ml of 2TY media containing 100 µg/ml ampicillin were grown at 30°C and induced at an optical density (600 nm) of 0.7 by adding IPTG to a final concentration of 1 mM. MFE-23 scFv was recovered from the filtered culture supernatant using ammonium sulphate precipitation by the addition of 1 L of 76% chilled ammonium sulphate solution followed by centrifugation at 10,000 g. The crude protein pellet was redissolved in binding buffer (phosphate buffered saline-PBS/0.5 M NaCl/1 mM MgCl₂ pH 8.0) and dialyzed against this buffer exhaustively. The crude protein was applied to a chelating Sepharose column charged with NiCl₂. The column was washed in binding buffer supplemented with imidazole 10–60 mM and the pure scFv was eluted in binding buffer with 100 mM imidazole.

C6.5 scFv was obtained from Prof. J. Marks (University of California, San Francisco) in pUC119 and expressed in XL1 blue cells.³¹ The C6.5 scFv was engineered to remove a lysine-100 in the antibody binding site. This was to reduce the possibility of forming PICs of reduced immunoreactivity.³¹ Cultures were grown as described earlier. Purification of C6.5 was carried out as described earlier for MFE-23.

Purified protein was either concentrated to 1 mg/ml protein using 25 ml spin concentrators and stored in 10% glycerol at -80°C, or used for couplings straight after purification without concentrating.

HuBC1 scFv (anti-EDB containing fibronectin) was constructed and expressed in pHEN2 (Harman *et al.*, unpublished work), F1 and GP6 (anti-human placental alkaline phosphatase (Dr. Wright, unpublished work) and D1.3³² were expressed in pHEN2. The expression and purification of all scFvs was the same as described earlier.

Synthesis of pyropheophorbide-*a* succinimidyl ester

Pyropheophorbide-*a* succinimidyl ester was synthesized for coupling to the scFv as follows. To a light protected solution of the pyropheophorbide-*a* (50 mg, 0.094 mmol) in a mixture of dry dichloromethane/tetrahydrofuran (DCM/THF) (9:1) *N*-hydroxysuccinimide (12.9 mg, 0.11 mmol) was added followed by dicyclohexylcarbodiimide (DCC) (23.2 mg, 0.11 mmol). After stirring for 12 hr (at room temperature) under argon, the precipitated dicyclohexylurea was filtered off and the solvents removed. The crude product was taken up in a small volume of chloroform and precipitated by the addition of hexane. The precipitate was collected, washed well with hexane and the resulting crude product purified by column chromatography on silica gel eluting with 20% hexane in ethyl acetate (*R*_f 0.66). The isolated product was recrystallized from DCM/hexane to give pure succinimidyl ester in 70% yield. Pyropheophorbide-*a* sulfo-succinimidyl ester was prepared in an analogous way. To a light protected solution of pyropheophorbide-*a* (50 mg, 0.094 mmol) in anhydrous dimethyl formamide (DMF)

(1 ml), *N*-hydroxysulfosuccinimide (85 mg, 0.393 mmol) was added followed by 1-(3-dimethylaminopropyl)-3-ethylcarbodiimide (69 mg, 0.444 mmol). After stirring for 12 hr (at room temperature) under argon, the solvent was evaporated to dryness and the residue purified by column chromatography on silica gel eluting with 20% hexane in ethyl acetate (*R*_f 0.33) to give a yield of 52%.

Synthesis of benzoporphyrin derivative (verteporfin) succinimidyl ester

The verteporfin succinimidyl ester was prepared as described for PPA. To a light-protected solution of verteporfin (6 mg, 0.0084 mmol) in anhydrous THF (5 ml), *N*-hydroxysuccinimide (3 mg, 0.0261 mmol) was added followed by DCC (6 mg, 0.0291 mmol). The reaction mixture was stirred for 12 hr (at room temperature) under argon when thin-layered chromatography (TLC-silica gel:ethyl acetate) confirmed consumption of all the starting material. The reaction mixture was evaporated and the residue purified by column chromatography on silica gel. The crude was loaded on to the column dissolved in the minimum of DCM and eluted with ethyl acetate (*R*_f 0.74) to give pure verteporfin succinimidyl ester in 75% yield.

Synthesis of scFv-photosensitizer photo-immunoconjugates (PICs)

The photosensitizer succinimidyl ester was resuspended in 100% DMSO and added at a concentration of 52.8 µM to 3.3 µM scFv in PBS containing 6% acetonitrile and with continuous stirring at 4°C for 30 min. The photoimmunoconjugates (PICs) were then dialyzed against PBS/2% DMSO with two buffer changes. For comparison of C6.5, F1, GP6 and D1.3, the concentrations of all the scFvs were adjusted so as to be the same as GP6 which gave the poorest expression of all the scFvs. There was no precipitation of the protein before coupling and the scFv-PPa conjugate remained soluble at concentrations of 0.25 mg/ml or below. Sodium dodecyl sulphate polyacrylamide gel electrophoresis (SDS-PAGE) analyses was carried and stained with coomassie blue. Nonstained gels were transferred using a semidry blotting apparatus (Biorad) onto nitrocellulose and gently dried. Fluorescence was visualized by exciting the PPA on the blot on a short wavelength UV-transilluminator. Figures 1a and 1b shows an example coupling and a calculation to determine the PPA:scFv ratio. The absorbance of 200 µg/ml PPA in PBS/2% DMSO gave an absorbance of 0.32 units at 670 nm (Fig. 1a). Thus 0.1 AU (found in a typical conjugate) is equal to 62.5 µg/ml PPA which is equal to 1.17×10^{-4} M PPA (molecular weight-*M*_w = 535). This was found coupled to a scFv at a concentration of 250 µg/ml (see Fig. 1b), which is equal to 8.3×10^{-6} M (*M*_w = 30,000). The ratio works out to be 14.1:1, which becomes 9.9:1 after correcting for 30% noncovalent binding (Fig. 2). Higher concentrations (0.5 mg/ml or 16.5 µM scFv) of PPA PICs were possible to obtain using the more aqueous soluble pyropheophorbide-*a* sulfo-succinimidyl ester. The coupling mixture was 264 µM pyropheophorbide-*a* sulfo-succinimidyl ester:16.5 µM scFv equivalent to the 16:1 ratio described earlier. This ratio includes covalently coupled and non-covalently bound photosensitizer. To apply a correction factor to determine the true PS:scFv ratio, SDS-PAGE gels were run and transferred to nitrocellulose. These blots were imaged under UV light in a FujiFilm[®] LAS-3000 imager where the coupled PS (migrating at the molecular weight of the scFv) and the free PS (migrating much more quickly) was visible as a fluorescent band. Using the manufacturers' software, densitometry was used to calculate the relative intensities/band sizes. This ratio was used to correct for noncovalent binding.

Spectroscopic measurements

The absorbance profile of the free photosensitizer (dissolved in 100% dimethyl sulphoxide-DMSO) and photosensitizer coupled to the scFv (dissolved in PBS/2% DMSO) was determined on a Hewlett Packard UV-Visible spectrophotometer. The number of Pyropheophorbide-*a* molecules attached to the scFv was deter-

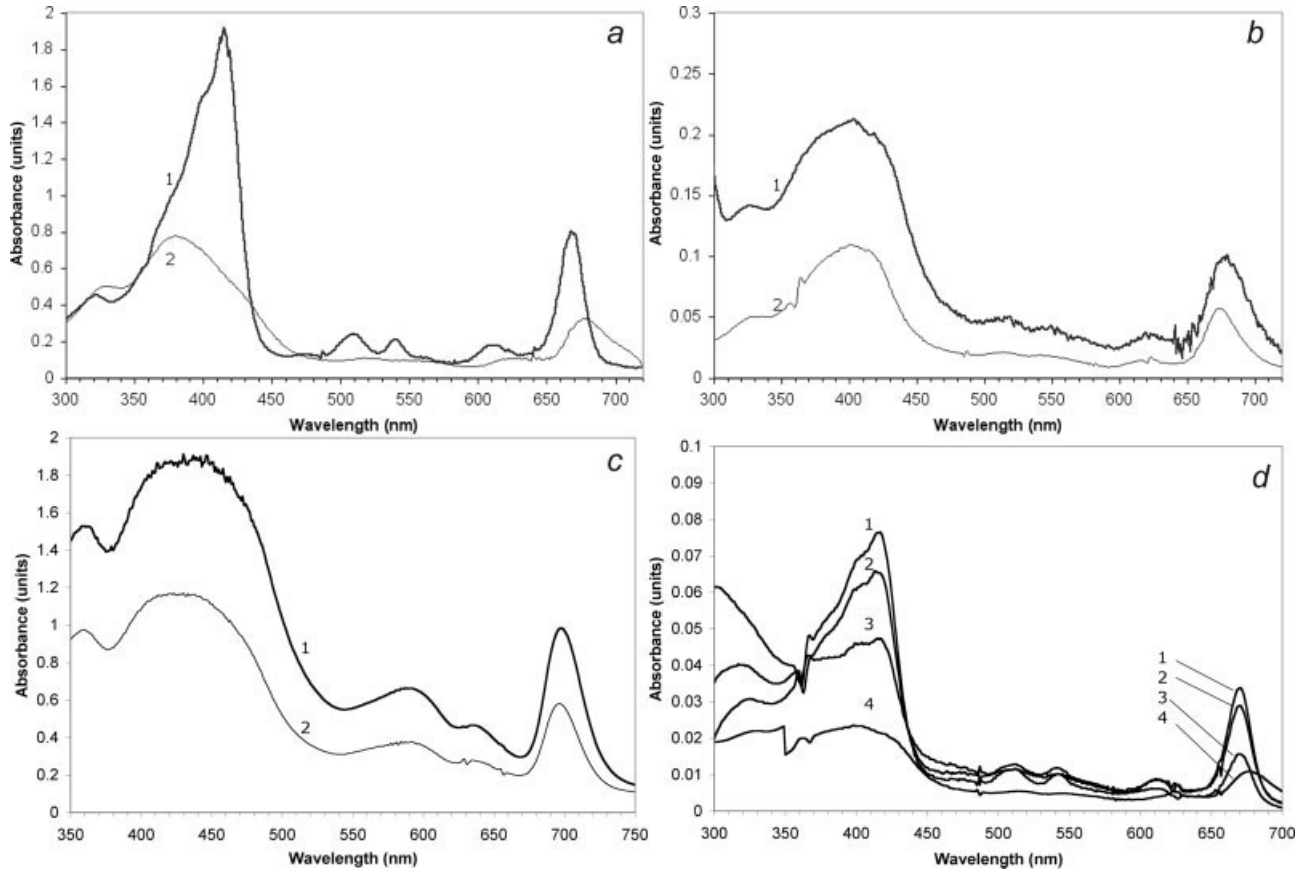


FIGURE 1 – Absorbance spectra of photosensitiser (PS) and scFv-PS photo immunoconjugates. (a) PPa-200 µg/ml in DMSO [1] and 200 µg/ml in PBS/2% DMSO [2]. (b) C6.5-PPa (250 µg/ml in PBS/2% DMSO) [1] and MFE-PPa (50 µg/ml in PBS/2% DMSO) [2]. (c) Verteporfin (VP) (50 µg/ml in PBS [1] and C6.5-VP [2] (200 µg/ml in PBS). (d) A panel of alternative scFv-PPa PICs all at 10 µg/ml, D1.3 [1], F1 [2], GP6 [3] and HuBC-1 [4].

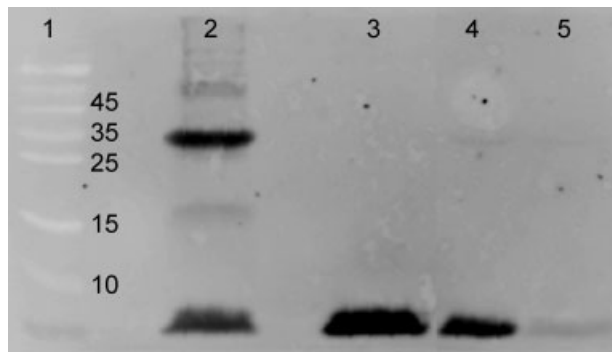


FIGURE 2 – SDS-PAGE blot analysis of C6.5-PPa photoimmunoconjugates C6.5 scFv after various coupling conditions was analyzed by fluorescence imaging after UV illumination. (1) Protein markers. (2) C6.5 scFv after full coupling with PPa active ester. (3) C6.5 scFv after mock coupling with PPa methyl ester. (4) Free PPa. (5) Free C6.5 scFv.

mined using the absorbance at 410 nm and 670 nm and compared to a standard curve of pyropheophorbide-*a*.

The singlet oxygen quantum yields of the photoimmunoconjugates were determined by direct measurement on aerated samples of the lyophilized immunoconjugate dissolved in D₂O/DPBS. A frequency-tripled Nd:YAG (neodymium-doped yttrium aluminium garnet-Continuum Powerlite 8000) pumped dye laser

(Lambda Physik 2002, Coumarin 120 laser dyes) was used as the pump source providing 0.01–2 mJ pump pulses at 420–460 nm, *ca* 10 ns duration. Singlet oxygen (¹O₂) generation was detected by its phosphorescence at 1270 nm using a North Coast Scientific EO-817P germanium photodiode detector. Quantum yields of ¹O₂ (Φ_{Δ}) of the photoimmunoconjugates were determined directly by the time-resolved infrared luminescence method as previously described.³³ The principle of this method is to measure the intensity of the photosensitized generated steady-state luminescence of singlet oxygen at 1270 nm of the sample and standards. The singlet oxygen quantum yields are calculated by comparison of the slopes of the energy dependence plots for luminescence emission for sample and standard. Optically matched samples of the lyophilized immunoconjugate were dissolved in D₂O/DPBS using TPPS4 ($\Phi_{\Delta} = 0.7$) and TMPyP ($\Phi_{\Delta} = 0.7$) in D₂O as standards.³⁴

In vitro cytotoxicity of scFv-PPa PICs

Cells were trypsinized and seeded at 2×10^4 cells/well into 96-well plates and incubated overnight at 37°C and 5% CO₂. The next day, the cells were washed once in PBS and 50 µl of the PICs (appropriately diluted) or free PPa were added to the appropriate wells under subdued lighting. PBS was added to control wells. After 30 min incubation in the dark at 37°C, 5% CO₂, cells were washed 3 times with PBS and 50 µl of PBS was added to each well. Wells were exposed to light from a 35 mW laser module (680 nm; Laser 2000, Northants, UK) at an energy dose of 4.2 J and an energy density of 13.4 J/cm² (control wells had either scFv-PPa or free PPa added and no exposure to light, or PBS added and exposure to light. Cells that had no scFv-PS or PS

added and no exposure to light were included as overall controls). Cells were incubated in the dark at 37°C, 5% CO₂ for 48 hr after which time, a cell titer assay was performed according to the manufacturer's instructions. The Promega Cell Titre-96™ system was used which involves the conversion by live cells of a tetrazolium compound (MTS) into a formazan dye which is measurable by its absorbance at 492 nm. For C6.5 containing PICs, SKOV-3 cells were used as the antigen (HER2) positive cell line and LoVo or KB cells used as the antigen negative cell line. For HuBC1-PPa, the same procedure as described earlier was used, but this time, WI38(VA13) cells were used as a positive cell line and SKOV-3 cells as a negative cell line.

In vivo experiments

ScFv, PPa and scFv-PPa (prepared as described earlier) were dialyzed into PBS and radiolabeled with Iodine-125 using the IODO-GEN® method (following the manufacturer's instructions). Briefly, Na¹²⁵I was activated (oxidized) by a brief incubation in Iodogen-coated tubes followed by mixing with the proteins to be radiolabeled. Free iodine was removed by a desalting column. The halogenation of porphyrins has been the subject of many reports.³⁵ The radiolabeling of PPa with ¹²⁵I is expected to proceed by electrophilic attack (by I⁺) on to the porphyrin periphery at the olefin or the sterically demanding 5-meso position. The iodination was carried out using ¹²⁵I, a methanolic solution of the porphyrin in an iodogen tube. After allowing to stand for 7 min, the mixture was passed through a Sep-Pak cartridge eluting with methanol, to remove the iodinating agent followed by the iodinated PPa (observed as a visible green band (radioactive)). The methanol was evaporated and the product reconstituted in PBS.

Four to 5 BALB/C nude mice (6–8 weeks old) per time point were injected in the tail vein with 5–10 µg ¹²⁵I labelled PPa, scFv or scFv-PPa. Mice were culled by cardiac puncture under terminal anaesthesia and blood and tissue samples were collected by dissection at 0.25, 1, 2, 3, 6 and 24 hr. The amount of radiolabeled scFv, PPa or scFv-PPa present was determined by γ -radiation counting and compared to the initial injected dose. The free PPa photosensitizer did not radiolabel as efficiently as the protein samples.

For therapy experiments 4–6 BALB/C nude mice (6–8 weeks old) per group were inoculated with 10 million SKOV3 tumor cells subcutaneously on the flank of the mice. Mice were treated 4–6 weeks later when the tumors had reached a diameter of 4–6 mm (volume of ~60 mm³). The volumes were calculated as width \times length \times width/2. Test mice were injected (i.v.) with 0.2 ml sterile, filtered PBS or 0.2 ml of 100–500 µg/ml C6.5-PPa under low light. It was calculated that 100 µg/ml C6-PPa at a 1:8 ratio contained 13 µg/ml net PPa. This was used for the free PPa control experiments. After 8–24 hr, mice were anaesthetized and placed on a warmed mat under a High Powered Devices (HPD) laser light set to 0.5 W at 670 nm. The mice were illuminated for 10 min at an energy dose of 110 J/cm². The mice were monitored during recovery and tumors measured 2–3 times per week. The growth delay or regression was compared between the 3 groups, by calculating the area under the curve for each animal as described by Matthews *et al.*³⁶ Analysis of variance was then used to compare the mean AUC between the groups. All *in vivo* experiments were carried out under a UK Home Office licence 70/5833.

Results

Photophysical properties of scFv-PPa PICs

The absorbance profile of free PPa and antibody-conjugated PPa is shown in Figures 1a, 1b, and 1d. All show the characteristic peaks around 400 nm (Soret band), minor peaks between 500 and 630 nm and an intense absorption around 670 nm, which is characteristic of chlorins (Q bands). Figure 1a shows PPa in DMSO where it retains its very sharp peaks and in PBS/2% DMSO cosolvent which is comparable to the buffers used for antibody conju-

TABLE I – PPa: scFv COUPLING RATIOS

ScFv	Specificity	PPa:scFv ratio
C6.5	HER2	8.3
MFE-23	CEA	6.0
D1.3	Hen Lysozyme	6.1
F1	Placental alkaline phosphatase	5.1
GP6	Placental alkaline phosphatase	3.1
HuBC-1	ED-B Fibronectin	2.1
C6.5	HER2	8.0 (VP ratio)

Effective photosensitizer: scFv coupling ratios determined by comparison to a PPa or verteporfin standard curves and correcting for 20–30% non-covalent binding. See Methods for example calculation.

gation. The absorbance of PPa in PBS/2% DMSO at the Q-band was used as a standard for PPa determination in the conjugates. Figure 1b shows the profile for the C6.5 scFv coupled to PPa measured in PBS/2% DMSO. The peaks have broadened slightly compared to that of DMSO-solubilized PPa with a 3–5 nm red-shifted 670 nm peak like PPa in aqueous buffers. This peak at around 670 nm was used to determine the PPa:scFv ratio which was 12.3 ± 1 (mean of 5). This gives an effective ratio of ~8.6:1 after correction for 30% (determined by densitometry) of non-covalent binding. The poor solubility of PPa limited PIC concentrations to around 0.25 mg/ml. Higher concentrations of C6.5-PPa PIC were obtained using the pyropheophorbide-*a* sulfosuccinimidyl ester which gave similar coupling results with no problems of protein aggregation (data not shown). The profile of PPa when attached to the control scFv MFE is also shown in Figure 1b. The ratio of PPa:MFE was 6:1. The C6.5 scFv was also coupled in the same way as described earlier to verteporfin (the active photosensitizer in the commercial drug Visudyne®) calculations giving a coupling ratio of 8:1 after correction for a lower degree of non-covalent binding (data not shown).

To confirm covalent attachment of the PPa onto the C6.5 scFv, SDS-PAGE gels were run and blotted onto nitrocellulose (Fig. 2). Under UV illumination, free and conjugated PPa fluoresced confirming covalent coupling and allowing the level of noncovalent binding to be determined. This coupling was absent when a non-reactive PPa methyl ester replaced it. Some free PPa, noncovalently associated with the protein is also seen. Densitometry measurements indicated that about 30% of the PPa was free. Both the scFv-PPa and free PPa fluoresced under UV illumination as expected for this photosensitizer. Singlet oxygen quantum yields (data not shown) for free PPa and C6.5-PPa were determined to be 0.26 and 0.25, respectively, indicating that the coupled PPa was functioning photophysically as effectively as free, aqueous PPa with little quenching occurring between sensitizer molecules.

Four further scFvs were coupled to PPa to understand those factors important in obtaining good coupling ratios (Fig. 1d). D1.3 scFv-PPa gives close to the "ideal" absorbance pattern exemplified by the C6.5 scFv, F1 scFv-PPa is slightly less effective. However, GP6 scFv-PPa and HuBC-1 scFv-PPa show poor profiles with broadened peaks, indicating possible aggregation. The ratio of PPa:scFv for all scFv coupling experiments are shown in Table I.

Targeted cellular cytotoxicity of the scFv-PPa PICs

Free photosensitizers were cytotoxic to cultured cells, in the presence of light. When KB and SKOV-3 cells were treated, PPa was more effective in killing the KB cells with a PPa IC₅₀ of 41 µM, whereas the IC₅₀ was 93 µM for the SKOV-3 cells. Verteporfin was a significantly more potent sensitizer on the same cell lines (IC₅₀ of 10.6 and 5.4 µM, respectively) (Fig. 3a). The C6.5-PPa (anti-HER-2) and MFE-23-PPa (anti-CEA) PICs were each tested on their antigen-negative and antigen-positive cell lines (SKOV-3-HER2+, CEA–), (LoVo-CEA+, HER2–). Each PIC was able to kill its respective receptor-expressing cell line and spare the receptor-negative cell line (Figs. 3b and 3c). C6.5-PPa killed cells

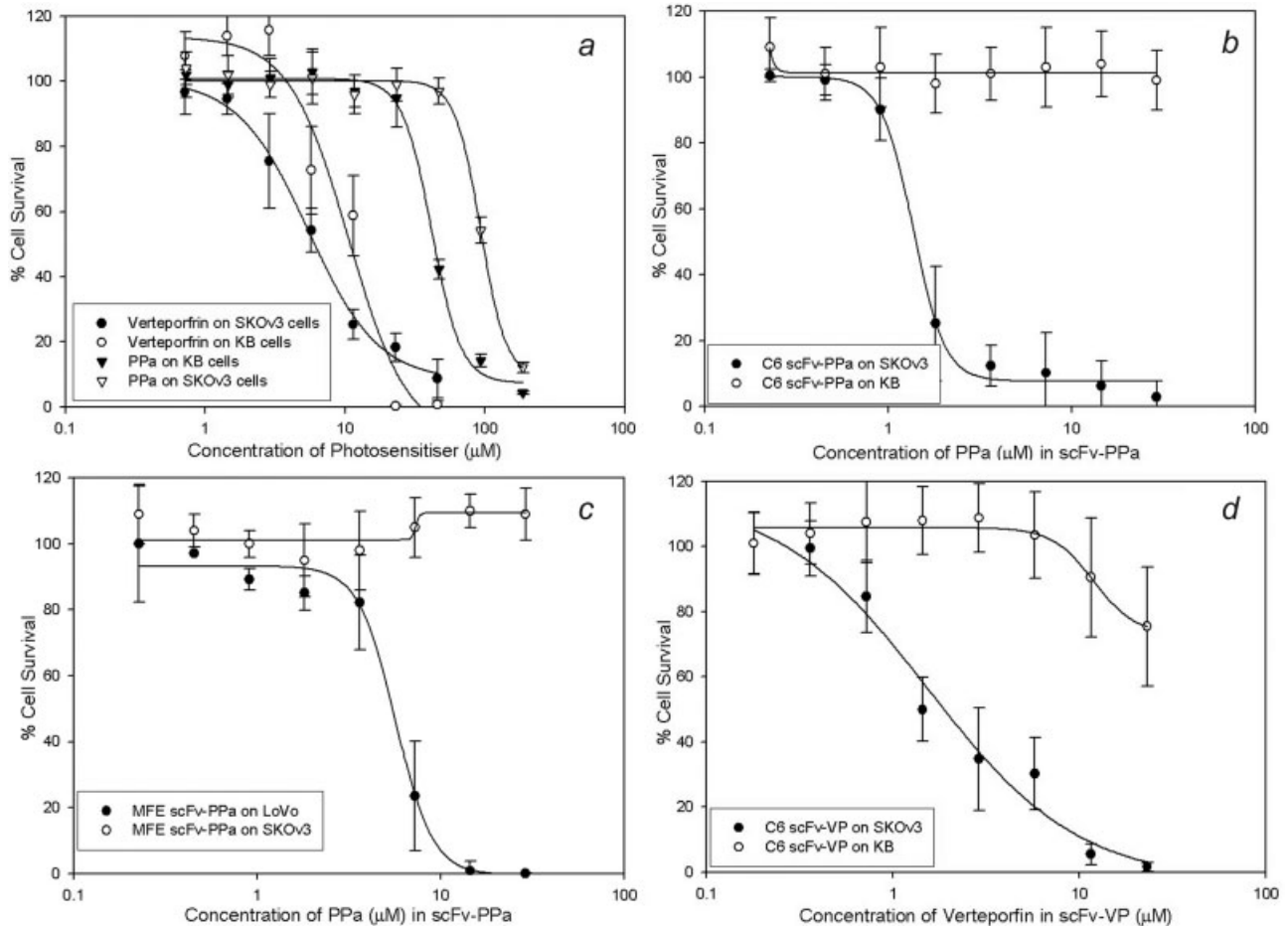


FIGURE 3 – *In vitro* cytotoxicity of scFv-PS photoimmunoconjugates. (a) Free photosensitisers on HER-2 positive (SKOV-3) and HER-2 negative (KB) cell lines. Verteporfin (VP) on SKOV-3 (●) and KB (○). PPa on KB (▼) and SKOV-3 (▽). (b) C6.5-PPa exposed to SKOV3 cells (●) and KB cells (○). (c) MFE scFv-PPa exposed to LoVo cells (●), MFE scFv-PPa exposed to SKOV3 cells (○). (d) C6.5-VP exposed to SKOV3 cells (●) and KB cells (○).

with a net PPa IC_{50} of 1.5 μM (Fig. 3b). The IC_{50} for MFE-PPa was 5.7 μM (Fig. 3c). Targeted verteporfin was more than 8-times more specific for the HER-2 expressing cell line compared to the antigen-negative cell line (IC_{50} of 1.4 μM compared to >12 μM), but despite this improvement in targeting, there was some nonspecific cell killing not observed with targeted PPa (Fig. 3d). There was no effect on the cell viability of any cell lines with light alone or scFv-PPa and PPa in the absence of light (data not shown). Cytotoxicity experiments were also carried out with HuBC1-PPa at the highest concentration of scFv (3.3 μM , 2:1 ratio) which gave 30% cell kills using the fibronectin positive cell line (WI38-VAI3) and no kills with the negative cell line, SKOV3 (data not shown). All the *in vitro* cytotoxicity results are summarized in Table II.

In vivo pharmacokinetics, biodistribution and therapy

The pharmacokinetic profile studies in nude mice are shown in Figure 4 with a summary of the kinetic values shown in Table III. Both species of scFv tested (C6.5 and MFE-23) demonstrated typical biphasic exponential clearance profiles with both showing an initial rapid α or distribution phase, followed by a slower β or deposition phase. The blood clearance of whole IgG ($t_{1/2\alpha} = 1.1$ hr and $t_{1/2\beta} = 76.2$ hr) and free PPa ($t_{1/2\alpha} = 1.6$ hr and $t_{1/2\beta} = 20.9$ hr) are relatively slow, because of their size and hydrophobicity, respectively. The clearance of the free scFvs are rapid as expected ($t_{1/2\alpha} = 0.12$ –0.13 hr and $t_{1/2\beta} = 4.1$ –4.4 hr). The two scFv-based PICs show pharmacokinetic profiles in between

that of free PPa and scFv ($t_{1/2\alpha} = 0.16$ –0.17 hr and $t_{1/2\beta} = 9.2$ –12.3 hr). The 4–5 kDa additional molecular weight possessed by the PICs is not enough to account for the significant reduction in blood clearance compared to the free scFvs and is likely due to the increased hydrophobicity of the PICs.

Biodistribution studies of the C6.5-PPa PIC indicated that a tumor:blood ratio of greater than approximately 3:1 was seen after 8 hr and $\sim 7:1$ (and significantly higher compared to other normal tissues) was achieved by 24 hr (Fig. 5). Some spleen uptake was seen, but the other tissues remained relatively clear. The targeting of the C6.5-PPa PIC was almost as effective as the free scFv (Fig. 5), but because of its slower clearance, the specificity ratios were lower. However, compared to free PPa there was more specific targeting and lower levels in all tissues (data not shown). Typically, the tissue levels of free PPa mirrored that of the blood levels (Fig. 4) with 20–30%/id/g at 8 hr and 10–15% id/g at 24 hr with high amounts in the spleen. On the basis of this data, PDT treatment cycles were tested on small tumors (3–5 mm in diameter) grown as xenografts. Tumor-bearing mice were injected with PBS-saline (untreated) or 20–100 μg of PIC (treated) 8 or 24 hr before laser illumination. One cycle and 3 cycles of treatment were tested. The progression of the tumors was followed and the results are shown in Figure 6. One cycle of treatment with 20 μg PIC followed 24 hr later by laser illumination was enough to cause tumor growth delay (data not shown). However, more significant differences between targeted PPa and non-targeted PPa was seen when the laser step was carried out 8 hr after PIC administration

TABLE II – *IN VITRO* CYTOTOXICITY OF PHOTOIMMUNOCONJUGATES

	Antigen expressed	IC ₅₀ (μM scFv)	IC ₅₀ (μM PS)
PPa on SKOV3 cells	HER2+, CEA–	NA	93
PPa on KB cells	HER2–	NA	41
C6.5-PPa on SKOV3 cells	HER2+, CEA–	0.16	1.3
C6.5-PPa on KB cells	HER2–	>3.1	>25
MFE-PPa on LoVo cells	CEA+, HER2–	0.95	5.7
MFE-PPa on SKOV3 cells	CEA–	>3.1	>25
VP on SKOV3 cells	HER2+	NA	5.4
VP on KB cells	HER–	NA	10.6
C6.5-VP on SKOV3 cells	HER2–	0.18	1.4
C6.5-VP on KB cells	HER2–	>3.1	>25

The IC₅₀s are expressed in terms of scFv protein concentration and effective photosensitizer concentration.

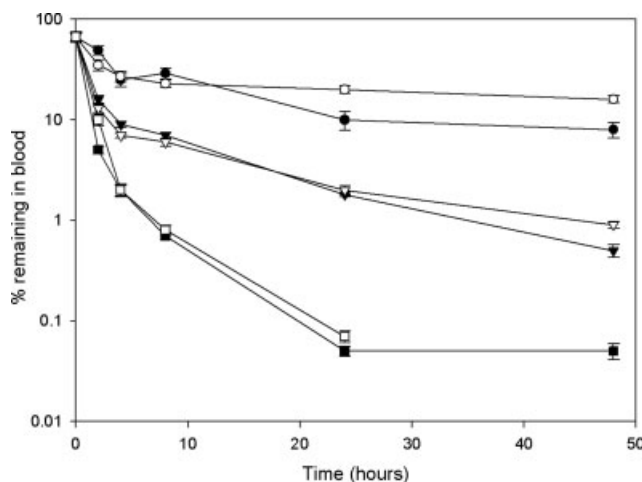


FIGURE 4 – Blood pharmacokinetics. The fraction remaining in the blood more than a period of 48 hr was measured for antibodies, PPa and photo-immunoconjugates. Radioactivity was followed for the radiolabelled species. Whole IgG (○), free PPa (●), C6.5-PPa (∇), MFE-PPa (▼), free C6.5 scFv (□) and free MFE scFv (■).

(Fig. 6a) which was improved when 100 μg was administered (Fig. 6b). At the higher dose some of the mice in the group underwent complete tumor eradication (data not shown). Multiple treatment cycles resulted in the whole group of animals being cured of tumors when 100 μg of PIC was administered in each cycle (Fig. 6c).

Discussion

The data presented here clearly show that it is possible to overcome the limitations in antibody-photosensitizer coupling resulting in the generation of efficient PICs which can kill tumors *in vivo*. We have found that the choice of coupling conditions and scFv sequence are fundamental to achieving high photosensitizer:scFv ratios. Many different cosolvent conditions were examined but the described conditions afforded a small window where both the scFv and PS were able to react optimally. Coupling of all scFvs to the activated PSs was performed in an aqueous buffer containing 1.9% DMSO and 6% acetonitrile as cosolvent. This retained the solubility of the scFv, and allowed the hydrophobic PSs to remain in solution long enough for the reaction to proceed. Significant aggregation problems were seen when pyropheophorbide-*a* succinimidyl ester was used at concentrations above 60 μM. This restricted the concentration of C6-PPa to 100 μg/ml. However, 5 times higher PICs were possible using a pyropheophorbide-*a* sulfo-succinimidyl ester in the same coupling reaction conditions. This highlights the importance developing PSs which make good PICs rather than stand-alone PSs. Counterintuitively, we have achieved higher direct coupling ratios on small antibody fragments than has been achieved with whole antibodies. More-

TABLE III – *IN VIVO* PHARMACOKINETIC PARAMETERS

Molecule	t _{1/2} (α) [hr]	t _{1/2} (β) [hr]
IgG	1.1	76.2
PPa	1.6	20.9
C6.5scFv	0.14	4.1
MFE-23 scFv	0.13	4.4
C6.5-PPa PIC	0.17	12.3
MFE-23-PPa PIC	0.16	9.2

The data from Figure 5a was fit to a bi-phasic exponential clearance curve and half-lives for the α- and β-phases were determined.

over, this has been realized without the need for additional chemical manipulations of the antibody (*e.g.*, PEGylation).³⁷ Our coupling conditions are far less harsh than those previously described by others where high concentrations of organic solvents are used³⁷ which greatly expands the potential utility of this technology. We also coupled a commercial photosensitizer, verteporfin (Visudyne[®]) and achieved results as good as that seen with PPa (Figs. 1 and 2). This allowed us to compare *in vitro* our technology with a “gold standard” photosensitizer. Previously verteporfin PICs consisting of an EGFR (epidermal growth factor receptor-1) recognizing MAb C225 were found on a per mole basis to be significantly less phototoxic than free visudyne.¹⁶

It is known that in the presence of aqueous buffers such as PBS, hydrophobic photosensitizers have a tendency to aggregate with consequent photophysical quenching.³⁸ The singlet oxygen data therefore strongly suggest that the PPa molecules are spatially arranged on the scFv such that there is less adverse photophysical interaction between PS molecules. This prompted us to investigate other scFvs as candidates for PS carriers. The variation in coupling efficiencies directed us to look more closely at the sequence and structure of the scFvs. It is clear that accessible surface lysine residues are essential for efficient coupling of PS, but the positioning also seems to be important. Sequence alignment (Fig. 7) of the scFvs used in this study revealed that C6.5, which gives reproducible coupling and good singlet oxygen yields has more lysines which (assuming that lysine residues tend to be at the surface of proteins rather than buried) are predicted to be spatially separated compared with scFvs which make poorer PICs (HuBC-1, GP6 and F1). A study where photosensitizers were coupled onto the surface of a dendrimer resulted in tightly packed and interacting photosensitizer molecules leading to a 10-fold reduction in singlet oxygen yield²¹ which supports our observations. Our coupling data suggest that the number and placement of lysines determines the suitability of the scFv as a PS carrier. This was demonstrated further by the scFv, HuBC1 coupled to PPa. The number of lysines available for coupling was 6, 2 of which are next to each other in the sequence, and the ratio of PS:scFv was found to be 2.1:1. This suggests that the 2 PS on the scFv are well-placed for coupling, but their positioning adversely affects their photophysics leading to insubstantial cell kills. Research by Bedouelle and coworkers³⁹ has also shown that the position of fluorophores coupled to scFvs is critical to the function of immunosensors with quenching by protein-protein interaction being required for an optical readout.

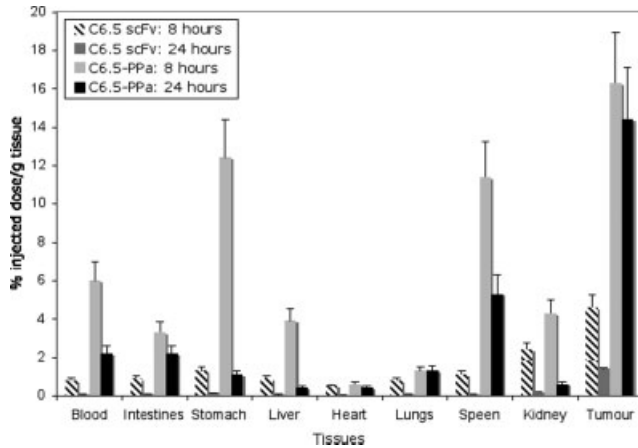


FIGURE 5 – Biodistribution of C6.5 scFv and C6.5-PPa PIC in tumor-bearing nude mice SKOV3 tumor-bearing nude mice (4 per group) were injected with 10µg of C6.5 scFv or C6.5-PPa PIC radiolabelled with ¹²⁵I. Tissues were dissected and counted at 8 hours and 24 hours. The percentage injected dose per gram of each major tissue is represented.

Our results are consistent with this observation in that lack of quenching by superficial spacing is important in generating the photodynamic effect. Therefore, the spatial arrangement of the lysines on the C6.5 scFv is ideal for the coupled PSs to produce reactive oxygen species that cause cell death. This is reflected in the *in vitro* and *in vivo* cell kill data. It seems likely that certain V-heavy and V-light domain protein sequences and structures are well-suited for *tPDT* (exemplified by the C6.5 scFv) and that poorer antibodies could be engineered to possess these enabling features.

In vitro cell killing using C6.5-PPa showed a greater than 70-fold enhancement of IC₅₀ over free PPa. This is in contrast to the work carried out by Sevallano *et al.*³⁷ using whole IgG against HER-2 coupled to PPa, which showed that free PS had a higher efficacy compared to using the coupled IgG-PPa. The dramatic differences in cell kill seen with our constructs compared to free PPa is a result of the loading and spatial arrangement of the PS on the scFv being conducive to minimal self-quenching and the fact that C6.5 is an internalizing antibody. Our work also showed that MFE-PPa gave a 7-fold enhancement over free PPa demonstrating that enhancement of tumor cell kill with our approach could be achieved with a different target.

Using HuBC1-PPa, on the other hand only gave 30% cell kills at the highest concentration of scFv-PPa, which was not surprising given the PPa:HuBC-1 scFv of 2:1.

We observed a much lower change in specificity on verteporfin (VP) coupling with the IC₅₀ for free VP against SKOV3 cells decreasing only 3.8-fold. Targeted VP was 8.4-fold more specific for antigen-expressing cells compare to a 2-fold difference in selectivity for nontargeted VP. This may be due to the differential cytotoxic profile of the conjugated VP compared to conjugated PPa. Nevertheless, this was the first demonstration of targeting and enhanced potency of this commercially applied photosensitizer.

Hydrophobic photosensitizers tend to have slow blood clearance because of the association with serum proteins. Whole antibodies have a slow clearance primarily due to their size. With a view to evaluating *tPDT in vivo*, we analyzed the pharmacokinetics of the scFv-PPa conjugates. The clearance of both the radio-labeled scFv and the scFv-PPa conjugate shows the characteristic biphasic pattern. The increased hydrophobicity of the scFv-PPa molecule switches the pharmacokinetic profile towards that of the free sensitizer. Despite this, the profile shows that the clearance is still more rapid than free PPa and whole antibody suggesting that the time from administration of the scFv-PPa to exposure to laser

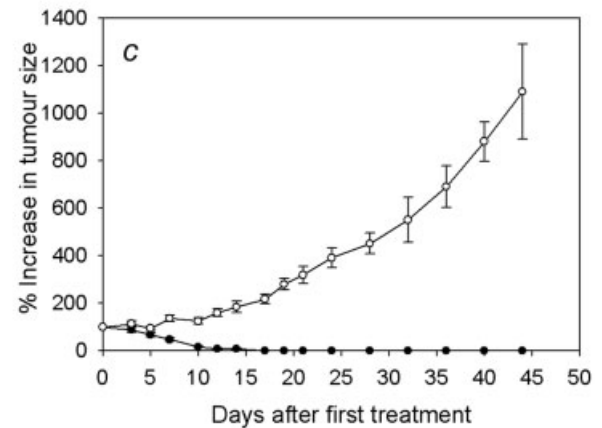
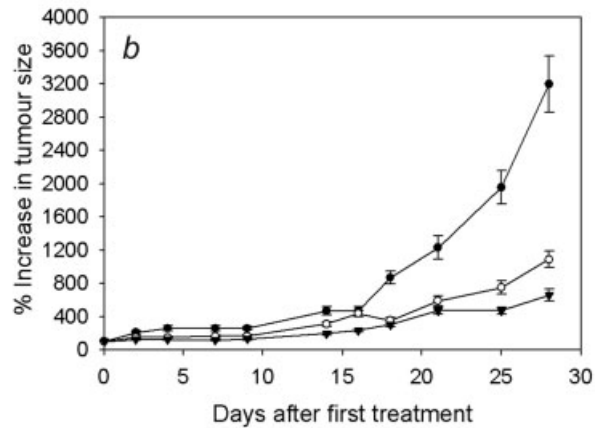
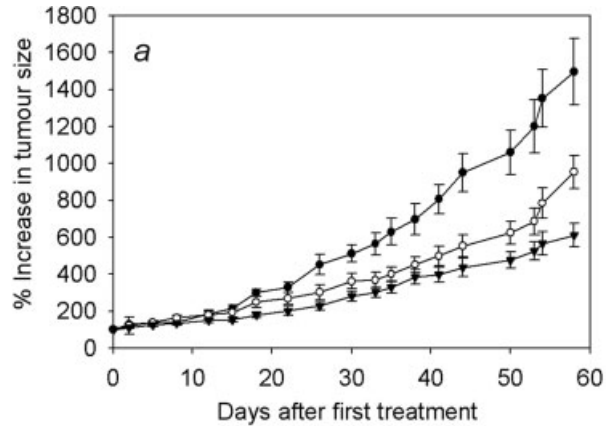


FIGURE 6 – PDT therapy experiments. (a) SKOV3 tumor-bearing nude mice (4 per group) were treated with PBS-saline (●), free PPa (○) and 20µg C6.5-PPa photoimmunoconjugate (▼) followed by laser illumination 8 hours later. The tumor growth progress was recorded over 2 months. (b) The experiment was repeated with 100µg of C6-PPa PIC. (c) Complete tumor regression was seen when comparing free PPa (○) and C6-targeted PPa (●) given in three doses at day 0, 7 and 14, followed by laser illumination after 8 hours. In all experiments, the free PPa was given at the same dose as that found in the C6-PPa PIC.

light could be therapeutically attractive with very little danger of skin photosensitivity.

Tumor treatment experiments verified that the C6.5-PPa conjugates are able to generate enough singlet oxygen *in vivo* and that a significant amount accumulated in the tumor to give substantial tumor regression. One dose cycle of PDT treatment caused good tumor regression. The dose administered was 20 µg mouse (~0.7

```

scFv Variable-heavy domain
GP6 EVQLVESGGGL-VQPGGSLRLSCAASGFTFSSYWMHWRQAPGKGLVWVSRINSDGSSAS
D1.3 QVQLQESGPGI-VAPSQSLITCTVSGFSLTGYGNWVRQPPGKGLEWLGMI-WGDGNTD
MFE QVKLQSQGAEL-VRSGETSVKLSCTASGFNIKDSYMHWLRQPEQGLEWIGWIDPENGDTG
F1 EVQLVQSGGGV-VQPGSLRLSCAASGFTFDDYGMWVRQAPGKGLEWVSGINWNGGSTG
BC-1 EVQLVQSGADV-KKPGASVKVSKASGYTFTNYVMHWRQAPGQGLEWLGYNINPYNDGTQ
C6.5 QVQLQSQGAEV-KKPGESLKISCKGSGYSFTSYWIAWVRQMPGKGLEWYMLIYPGSDSTK

scFv Variable-heavy domain
GP6 YADSVKGRFTISRDNAKNTLYLQMNLSRAEDTAVYYCAR-TVT-----ER
D1.3 YNSALKSRSLISKDNSKSOVFLKMNSLHTDDTARYYCARERDYR-----LDY
MFE YAPKFQGGKATFTTDSNTAYLQLSLSLSEDTAVYYCNEGTPTG-----PYFFDY
F1 YADSVKGRFTISRDNAKNSLFLQMNLSRAEDTALYYCAR-AIRSYSGS-----YGNAFDI
BC-1 YNERFKGRVTMTGDTISISTAYMELSRSLTSDTAVYYCAR-EVYG-----NYIWN
C6.5 YSPSFQGVVTSVSKSVSTAYLQWSSLKPSDSAVYFCAR-HDVGYCSSNCAKWEPEYFQH

scFv Linker Variable-light domain
GP6 WGQGTLVTVSS GGGGSGGGSGGSAL SSELTDQ-P-AVSVALGQTVRITCQGDLS--RSY
D1.3 WGQGTTVTVSS GGGGSGGGSGGSAL DIQMTQS-PASLSASVGETVTITCRASGN--IHN
MFE WGQGTTVTVSS GGGGSGGGSGGGGS ENVLTQS-PAIMSASPGKVTITCSASSS-VS--
F1 WGKGTLVTVSS GGGGSGGGSGGGGS DIQMTQS-PSTLSASIGDRVITITCRASEG--IYH
BC-1 WGQGTLVSVSS GGGGSGGGSGGSAL EIVLTQS-PGTLSPGERATLSCSASSS-ISSN
C6.5 WGQGTLVTVSS GGGGSGGGSGGGGS QSVLTQP-P-SVSAAPGQKVTISCSGSSSNIGNN

scFv Variable-light domain
GP6 YASWYQQKPGQAPVLIYG---KNNRPSGIPDRFSGS--SSGNTASLTITGAQAEDEAD
D1.3 YLAWYQQKQKSPQLLVYY---TTTLADGVPSRFSGS--GSGTQYSLKINSLQPEDFGS
MFE YMHWFQKPGTSPKLIWYS---TSNLAGVPARFSGS--GSGTSYSLTISRMEAEDAAT
F1 WLAWYQQKPGKAPKLLIYK---ASSLASGAPSRFSGS--GSGTDFTLTISLQPDFFAT
BC-1 YLHWYQQKPGQAPRLIYR---TSNLAGIPDRFSGS--GSGTDFTLTISRLEPEDFAV
C6.5 YVSWYQQLPGTAPKLLIYG---HTNRPAQVPSRFSGS--KSGTSASLAISGFRSEDEAD

scFv Variable-light domain
GP6 YYCNSRDS--SGTVFGGGTKLTVL
D1.3 YYCQHFWS--TPRTFGGGTKLEIQ
MFE YYCQQRSS--YPLTFGAGTKLEIK
F1 YYCQQYSN--YPLTFGGGTvLEIK
BC-1 YYCQQGSS--IPFTFGQGTKEIN
C6.5 YYCAAWDDSLSGWVFGGGTKLTVL

```

FIGURE 7 – Amino acid alignment of scFvs used in this study. The variable heavy-linker-variable light domains are shown with lysine residues highlighted in bold to illustrate the variability in number and position which may influence PDT coupling efficiency and photoimmunoconjugate potency.

mg/kg) which was lower than typical doses used by others.²³ The tumors chosen were around 5 mm in diameter which was well within the range of depth of penetration of the laser used. No skin photosensitivity was evident in the treated mice. Increasing the dose 5-fold led to a better overall tumor response with some mice being eradicated of tumor burden. But the best results were seen with 3 treatment cycles with the laser illumination being given at an earlier time point when there was more PIC in the tumor. It is likely that clinically, many treatment cycles would be needed to treat such comparatively large tumor masses. The 7-day timing has not been optimized and could be successful as it allows the apoptotic pathway to execute fully before the next treatment cycle. There is scope, however, to shorten this interval.

In conclusion, we can couple significantly more photosensitizers directly onto scFvs than previously achieved with whole antibodies, while maintaining the key photophysical properties required for efficient photodynamic efficacy as borne out by our *in vivo* therapy data. Furthermore, the number and distribution of lysine residues on the surface of the scFv may have a direct influence on the photophysical function of the PS coupled to them and has implications for the design of better photoimmunoconjugates.

Our PICs demonstrate improved pharmacokinetics and biodistribution compared to free photosensitizers and whole antibody-based PICs which should have implications for reducing side effects such as photosensitivity and thus providing considerable patient benefit especially as our method has the potential to be applied to existing clinically relevant photosensitizers.

Acknowledgements

We gratefully acknowledge Dr. Marina Kuimova, Ms. Ioanna Stamati and Prof. David Phillips (Imperial College London) for technical help and useful discussions. We would like to thank Dr. Richard Morris, UCL for statistical advice. M.P.D., L.R.M. and G.Y. are cofounders and minor shareholders in PhotoBiotics, an Imperial College spin-out company which funded this research. We thank Dr. Gregory Adams and Prof. James Marks for the C6.5 scFv and advice and we thank Dr. Nigel Courtenay-Luck (Antisoma Research, Ltd.) for the use of the huBC-1 scFv. We would also like to thank the European Union Framework 6 programme for additional funding, grant reference LSHC-CT-2006-037489, Immuno-PDT.

References

- Lou PJ, Jones L, Hopper C. Clinical outcomes of photodynamic therapy for head-and-neck cancer. *Technol Cancer Res Treat* 2003;2:311–17.
- Pervaiz S. Reactive oxygen-dependent production of novel photochemotherapeutic agents. *FASEB J* 2001;15:612–7.
- Brown SB, Brown EA, Walker I. The present and future role of photodynamic therapy in cancer treatment. *Lancet Oncol* 2004;5:497–508.
- Dolmans DE, Fukumura D, Jain RK. Photodynamic therapy for cancer. *Nat Rev Cancer* 2003;3:380–7.

5. Sanfilippo NJ, His A, DeNittis AS, Ginsberg GG, Kochman ML, Friedberg JS, Hahn SM. Toxicity of photodynamic therapy after combined external beam radiotherapy and intraluminal brachytherapy for carcinoma of the upper aerodigestive tract. *Las Surg Med* 2001;28:278–81.
6. Waidelich R, Hofstetter A, Stepp H, Baumgartner R, Weninger E, Kriegmair M. Early clinical experience with 5-aminolevulinic acid for the photodynamic therapy of upper tract urothelial tumours. *J Urology* 1998;159:401–4.
7. Wolfsen HC. Present status of photodynamic therapy for high-grade dysplasia in Barrett's esophagus. *J Clin Gastroenterol* 2005;39:189–202.
8. Cappugi P, Campolmi P, Mavilia L, Prignano F, Rossi R. Topical 5-aminolevulinic acid and photodynamic therapy in dermatology: a minireview. *J Chemother* 2001;13:494–502.
9. Hopper C, Niziol C, Sidhu M. The cost-effectiveness of Foscan mediated photodynamic therapy (Foscan-PDT) compared with extensive palliative surgery and palliative chemotherapy for patients with advanced head and neck cancer in the UK. *Oral Oncol* 2004;40:372–82.
10. Sickenberg M. Verteporfin therapy for subfoveal choroidal neovascularization in age-related macular degeneration: from clinical trials to clinical practice. *Semin Ophthalmol* 2001;16:207–12.
11. Kormeili T, Yamauchi PS, Lowe NJ. Topical photodynamic therapy in clinical dermatology. *Br J Dermatol* 2004;150:1061–9.
12. Dougherty TJ. Photodynamic therapy. *Photochem Photobiol* 1993;58:895–900.
13. van Dongen GA, Visser GW, Vrouwenraets MB. Photosensitizer-antibody conjugates for detection and therapy of cancer. *Adv Drug Deliv Rev* 2004;56:31–52.
14. Sharman WM, van Lier JE, Allen CM. Targeted photodynamic therapy via receptor mediated delivery systems. *Adv Drug Deliv Rev* 2004;56:53–76.
15. Embleton ML, Nair SP, Cookson BD, & Wilson M. Antibody-directed photodynamic therapy of methicillin resistant *Staphylococcus aureus*. *Microb. Drug. Resist.* 2004;10:92–97.
16. Savellano MD, Hasan T. Targeting cells that overexpress the epidermal growth factor receptor with polyethylene glycolated BPD verteporfin photosensitizer immunoconjugates. *Photochem Photobiol* 2003;77:431–9.
17. Hudson R, Carcenac M, Smith K, Madden L, Clarke OJ, Pelegrin A, Greenman J, Boyle RW. The development and characterisation of porphyrin isothiocyanate-monoclonal antibody conjugates for photoimmunotherapy. *Br J Cancer* 2005;92:1442–9.
18. Vrouwenraets MB, Visser GW, Loup C, Meunier B, Stigter M, Opeelaar H, Stewart FA, Snow GB, van Dongen GA. Targeting of a hydrophilic photosensitizer by use of internalizing monoclonal antibodies: a new possibility for use in photodynamic therapy. *Int J Cancer* 2000;88:108–14.
19. Vrouwenraets MB, Visser GW, Stewart FA, Stigter M, Opeelaar H, Postmus PE, Snow GB, van Dongen GA. Development of meta-tetrahydroxyphenylchlorin-monoclonal antibody conjugates for photoimmunotherapy. *Cancer Res* 1999;59:1505–13.
20. Molpus KL, Hamblin MR, Rizvi I, Hasan T. Intraperitoneal photoimmunotherapy of ovarian carcinoma xenografts in nude mice using charged photoimmunconjugates. *Gynecol Oncol* 2000;76:397–404.
21. Aveline BM, Hasan T, Redmond RW. The effects of aggregation, protein binding and cellular incorporation on the photophysical properties of benzoporphyrin derivative monoacid ring A (BPDMA). *J Photochem Photobiol B* 1995;30:161–9.
22. Batra SK, Jain M, Wittel UA, Chauhan SC, Colcher D. Pharmacokinetics and biodistribution of genetically engineered antibodies. *Curr Opin Biotechnol* 2002;13:603–8.
23. Chester KA, Bhatia J, Boxer G, Cooke SP, Flynn AA, Huhlov A, Mayer A, Pedley RB, Robson L, Sharma SK, Spencer DI, Begent RH. Clinical applications of phage-derived sFvs and sFv fusion proteins. *Dis Markers* 2000;16:53–62.
24. Birchler M, Viti F, Zardi L, Spiess B, Neri D. Selective targeting and photocoagulation of ocular angiogenesis mediated by a phage-derived human antibody fragment. *Nat Biotechnol* 1999;17:984–8.
25. Fabbri M, Trachsel E, Soldani P, Bindi S, Alessi P, Bracci L, Kosmehl H, Zardi L, Neri D, Neri P. Selective occlusion of tumour blood vessels by targeted delivery of an antibody-photosensitizer conjugate. *Int J Cancer* 2006;118:1805–13.
26. Adams GP, Schier R, Marshall K, Wolf EJ, McCall AM, Marks JD, and Weiner LM. Increased affinity leads to improved selective tumour delivery of single-chain Fv antibodies. *Cancer Res* 1999;58:485–90.
27. Haddad R, Kaplan O, Greenberg R, Siegal A, Skornick Y, Kashtan H. Photodynamic therapy of murine colon cancer and melanoma using systemic aminolevulinic acid as a photosensitizer. *Int J Surg Investig* 2000;2:171–8.
28. Cuenca RE, Allison RR, Sibata C, Downie GH. Breast cancer with chest wall progression: treatment with photodynamic therapy. *Ann Surg Oncol* 2004;11:322–7.
29. Muschter R. Photodynamic therapy: a new approach to prostate cancer. *Curr Urol Rep* 2003;4:221–8.
30. Begent RH, Verhaar MJ, Chester KA, Casey JL, Green AJ, Napier MP, Hope-Stone LD, Cushen N, Keep PA, Johnson CJ, Hawkins RE, Hilson AJ, et al. Clinical evidence of efficient tumour targeting based on single-chain Fv antibody selected from a combinatorial library. *Nat Med* 1996;2:979–84.
31. Adams GP, Shaller CC, Chappell LL, Wu C, Horak EM, Simmons HH, Litwin S, Marks JD, Weiner LM, Brechbiel MW. Delivery of the α -emitting radioisotope bismuth-213 to solid tumors via single-chain Fv and diabody molecules. *Nucl Med Biol* 2000;27:339–46.
32. Ward ES. Antibody engineering: the use of *Escherichia coli* as an expression host. *FASEB J* 1992;6:2422–7.
33. Spiller W, Kliesch H, Wöhrle D, Hackbarth S, Röder B, Schnurpfeil G. Singlet oxygen quantum yields of different photosensitizers in polar solvents and miscellar solutions. *J Porphyrins Phthalocyanines* 1998;2:145–58.
34. Wilkinson F, Helman WP, Ross AB. *J Phys Chem Ref Data* 1995;24:663–1021.
35. Boyle RW, Johnson CK, Dolphin D. Iodination and heck alkynylation of 5,15-diphenylporphyrin. A convenient entry to asymmetrically meso-substituted porphyrins. *Chem Commun* 1995;527–8.
36. Matthews JN, Altman DG, Campbell MJ, Royston P. Analysis of serial measurements in medical research. *BMJ* 1990;300:230–5.
37. Savellano MD, Pogue BW, Hoopes PJ, Vitetta ES, Paulsen KD. Multiepitope HER2 targeting enhances photoimmunotherapy of HER2-overexpressing cancer cells with pyropheophorbide-a immunoconjugates. *Cancer Res* 2005;65:6371–9.
38. Hackbarth S, Horneffer V, Wiehe A, Hillenkamp F, Roder B. Photophysical properties of pheophorbide-a substituted diaminobutane poly-propylene-imine dendrimer. *Chem Phys* 2001;269:339–46.
39. Renard M, Belkadi L, Bedouelle H. Deriving topological constraints from functional data for the design of reagentless fluorescent immunosensors. *J Mol Biol* 2003;326:167–75.